04-07 April 2007

TECH BRIEFS

NATIONAL AERONAUTICS AND SPACE ADMINISTRATION

INTRODUCTION

Tech Briefs are short announcements of innovations originating from research and development activities of the National Aeronautics and Space Administration. They emphasize information considered likely to be transferable across industrial, regional, or disciplinary lines and are issued to encourage commercial application.

Availability of NASA Tech Briefs and TSPs

Requests for individual Tech Briefs or for Technical Support Packages (TSPs) announced herein should be addressed to

National Technology Transfer Center

Telephone No. **(800) 678-6882** or via World Wide Web at **www2.nttc.edu/leads/**

Please reference the control numbers appearing at the end of each Tech Brief. Information on NASA's Innovative Partnerships Program (IPP), its documents, and services is also available at the same facility or on the World Wide Web at **http://ipp.nasa.gov**.

Innovative Partnerships Offices are located at NASA field centers to provide technology-transfer access to industrial users. Inquiries can be made by contacting NASA field centers listed below.

NASA Field Centers and Program Offices

Ames Research Center
Lisa L. Lockyer
(650) 604-1754
lisa.l.lockyer@nasa.gov

Dryden Flight Research Center
Gregory Poteat
(661) 276-3872
greg.poteat@dfrc.nasa.gov

Glenn Research Center
Kathy Needham
(216) 433-2802
kathleen.k.needham@nasa.gov

Goddard Space Flight Center
Nona Cheeks
(301) 286-5810
nona.k.cheeks@nasa.gov

Jet Propulsion Laboratory
Ken Wolfenbarger
(818) 354-3821
james.k.wolfenbarger@jpl.nasa.gov

Johnson Space Center
Michele Brekke
(281) 483-4614
michele.a.brekke@nasa.gov

Kennedy Space Center
David R. Makufka
(321) 867-6227
david.r.makufka@nasa.gov

Langley Research Center
Martin Waszak
(757) 864-4015
martin.r.waszak@nasa.gov

Marshall Space Flight Center
Jim Dowdy
(256) 544-7604
jim.dowdy@msfc.nasa.gov

Stennis Space Center
John Bailey
(228) 688-1660
john.w.bailey@nasa.gov

Carl Ray, Program Executive
Small Business Innovation Research (SBIR) & Small Business Technology Transfer (STTR) Programs
(202) 358-4652
carl.g.ray@nasa.gov

Doug Comstock, Director
Innovative Partnerships Program Office
(202) 358-2560
doug.comstock@nasa.gov

TECH BRIEFS

NATIONAL AERONAUTICS AND SPACE ADMINISTRATION

Wearable Environmental and Physiological Sensing Unit

Safety of operations in hazardous environments could be enhanced.

Ames Research Center, Moffett Field, California

The wearable environmental and physiological sensing unit (WEPS) is a prototype of systems to be worn by emergency workers (e.g., firefighters and members of hazardous-material response teams) to increase their level of safety. The WEPS includes sensors that measure a few key physiological and environmental parameters, a microcontroller unit that processes the digitized outputs of the sensors, and a radio transmitter that sends the processed sensor signals to a computer in a mobile command center for monitoring by a supervisor. The monitored parameters serve as real-time indications of the wearer's physical condition and level of activity, and of the degree and type of danger posed by the wearer's environment. The supervisor could use these indications to determine, for example, whether the wearer should withdraw in the face of an increasing hazard or whether the wearer should be rescued.

The sensed parameters are the temperatures inside and outside the wearer's protective suit, the wearer's pulse rate and level of oxygen saturation of hemoglobin, acceleration, and concentration of combustible gas in the air. The wearer's pulse rate and level of oxygen are sensed by a commercially available pulse/oximeter that is clipped to the wearer's ear. The pulse/oximeter sends red and infrared light of several wavelengths into the wearer's tissues and measures the pattern and intensity of the light as scattered by the wearer's tissues. A companion signal-processing electronic circuit processes the analog output of the pulse/oximeter into a digital stream that is sent to the microcontroller unit.

The temperatures inside and outside the protective suit are measured by thermocouples. The analog outputs of the thermocouple circuits are fed to analog-to-digital converters (ADCs) within the microcontroller unit. The temperature readings are obviously of value in sensing overheating of the wearer and assessing the level of external hazard during firefighting.

The pulse reading can be used to determine the wearer's panic level and estimate the rate of consumption of air if the wearer is breathing from a tank. The presence or absence of a pulse can be used to determine whether the wearer is still alive when the wearer is unconscious or otherwise unable to respond by radio. The oxygen level is a good indicator of the wearer's overall health and can aid in identifying a respiratory deficiency that could lead to unconsciousness.

The wearer's acceleration is sensed by a commercially available two-axis accelerometer, the analog outputs of which are sent via buffer amplifiers to ADCs in the microcontroller unit. The accelerometer readings are taken as indications of the wearer's motion and, hence, level of physical activity.

The combustible-gas sensor is a commercially available unit that contains a catalytic bead heated to a temperature (≈500 °C) at which it can oxidize combustible gases. The role of this sensor is to provide a warning when the concentration of combustible gas in the wearer's vicinity approaches the lower explosive limit. The temperature of the bead, which varies with the atmospheric concentration of combustible gas, is transduced to a voltage that is buffered and sent to the microcontroller unit.

The microcontroller unit combines all the digitized sensor readings into a single digital stream at a maximum data rate of 10 kb/s. The stream is used to modulate the carrier signal in the radio transmitter, which operates at a frequency of 433.92 MHz. A receiver in the mobile command station recovers the data stream and sends it to the serial port of a laptop computer equipped with software that recognizes the data streams of the individual sensors in the combined stream and generates a visual display of the data coming from each sensor.

This work was done by Stevan Spremo of Ames Research Center and Jim Ahlman, Ed Stricker, and Elmer Santos of San Jose State University.

Inquiries concerning rights for the commercial use of this invention should be addressed to the Ames Technology Partnerships Division at (650) 604-2954. Refer to ARC-14770-1.

Broadband Phase Retrieval for Image-Based Wavefront Sensing

Broadband light can be approximated as monochromatic in phase-retrieval computations.

Goddard Space Flight Center, Greenbelt, Maryland

A focus-diverse phase-retrieval algorithm has been shown to perform adequately for the purpose of image-based wavefront sensing when (1) broadband light (typically spanning the visible spectrum) is used in forming the images by use of an optical system under test and (2) the assumption of monochromaticity is applied to the broadband image data. Heretofore, it had been assumed that in order to obtain adequate performance, it is necessary to use narrowband or monochromatic light.

Some background information, including definitions of terms and a brief description of pertinent aspects of image-based phase retrieval, is prerequisite to a meaningful summary of the present development. "Phase retrieval" is a general term used in optics to denote estimation of optical imperfections or "aberrations" of an optical system under test. The term "image-based wavefront sensing" refers to a general class of algo-

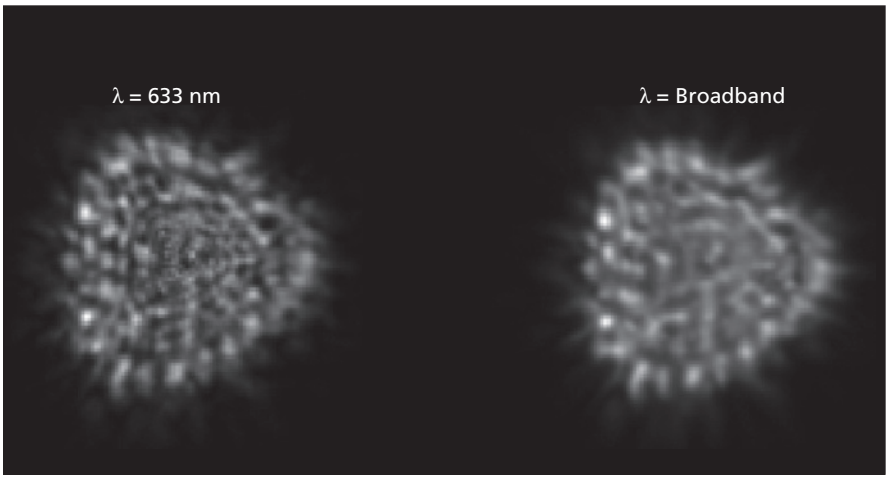

These **Point-Spread-Function Images** were obtained as the response of a test optical system (a deformable mirror) at the two noted wavelengths. The overall trefoil shape, representative of low-order aberrations, does not differ much between the two wavelengths. The "bumpy" higher-spatial-frequency image components of the two images differ noticeably, but these components represent higher-order aberrations that, typically, are smaller than the lower-order aberrations.

rithms that recover optical phase information, and phase-retrieval algorithms constitute a subset of this class.

In phase retrieval, one utilizes the measured response of the optical system under test to produce a phase estimate. The optical response of the system is defined as the image of a point-source object, which could be a star or a laboratory point source. The phase-retrieval problem is characterized as "image-based" in the sense that a charge-coupled-device camera, preferably of scientific imaging quality, is used to collect image data where the optical system would normally form an image. In a variant of phase retrieval, denoted phase-diverse phase retrieval [which can include focus-diverse phase retrieval (in which various defocus planes are used)], an additional known aberration (or an equivalent diversity function) is superimposed as an aid in estimating unknown aberrations by use of an image-based wavefront-sensing algorithm.

Image-based phase-retrieval differs from such other wavefront-sensing methods, such as interferometry, shearing interferometry, curvature wavefront sensing, and Shack-Hartmann sensing, all of which entail disadvantages in comparison with image-based methods. The main disadvantages of these non-image-based methods are complexity of test equipment and the need for a wavefront reference. This concludes the background information.

The present development began with a theoretical observation that the low-order aberration content of the point-spread-function of an optical system is not strongly affected by wavelength over the visible spectrum (see figure). As a result, variations in wavelength do not significantly affect what a phase-retrieval algorithm "sees" as input. This lack of variability of effective input is what makes it possible to assume monochromaticity when processing image data acquired while using broadband light.

The validity of the assumption of monochromaticity was demonstrated by comparing wavefront-sensing performances for broadband and monochromatic light in a known aberration test case. The significance of this development is that phase-retrieval algorithms can produce accurate phase estimates when test light is passed through filters having pass bands broader than were previously thought to be useable. Because more light is transmitted by broadband than by narrow-band filters, image-detector integration times can be significantly reduced and, therefore, time needed to perform wavefront sensing can be reduced. In some applications, filters can be eliminated entirely, thereby minimizing the complexity and cost of equipment for testing optical systems.

This work was done by Bruce H. Dean of Goddard Space Flight Center. Further information is contained in a TSP (see page 1).
GSC-14899-1

Filter Function for Wavefront Sensing Over a Field of View

Optical performance is more balanced when data from more field points are used.

Goddard Space Flight Center, Greenbelt, Maryland

A filter function has been derived as a means of optimally weighting the wavefront estimates obtained in image-based phase retrieval performed at multiple points distributed over the field of view of a telescope or other optical system. When the data obtained in wavefront sensing and, more specifically, image-based phase retrieval, are used for controlling the shape of a deformable mirror or other optic used to correct the wavefront, the control law obtained by use of the filter function gives a more balanced optical performance over the field of view than does a wavefront-control law obtained by use of a wavefront estimate obtained from a single point in the field of view. (The terms "wavefront sensing," "image-based," and "phase retrieval" are defined in the immediately preceding article.)

In a conventional approach to sensing and control of wavefronts, optical phase errors are estimated from the image of a single star or equivalent point source of light at a specific single location on a focal-plane image sensor. In effect, a wavefront control law is derived from a small area surrounding a single field point and is subsequently used to correct the performance of the optical system over the entire field of view. The disadvantage of this approach is that the performance of the system at other field points can suffer additional degradation because the wavefront information obtainable at those field points can differ from that obtained at the chosen field point.

A mathematically complete description of the filter function and its derivation would exceed the space available for this article; it must suffice to summarize. The derivation of the filter function

begins with the concept of an anisoplanatic function, defined as a phase function representative of the degree to which imaging performance varies over the field of view. The wavefront phase at a given field point is assumed to be given by the sum of the isoplanatic and anisoplanatic contributions. It is further assumed that an estimate of an isoplanatic phase function at a given field point can be modeled as a sum, over all other field points, of the convolutions of the filter function with the wavefront phase. Then the filter-function problem is formulated as one of choosing the filter coefficients to minimize the sum, over all field points, of the squares of the differences between the estimated and exact phase values of the isoplanatic phase function. To minimize this sum, one sets the partial derivatives of this sum with respect to the filter coefficients equal to zero. After some further algebraic manipulations, one obtains equations for the filter coefficients and an equation for the corrected wavefront generated by use of the filter function.

The filter function was tested in a computational simulation based on the optical design of the James Webb Space Telescope. Among the results, the variation of phase error over the field of view was 83 percent less in the case of a multiple-field-point/filter-function control law than in the case of a single-field-point control law (see figure).

This work was done by Bruce H. Dean of Goddard Space Flight Center. Further information is contained in a TSP (see page 1).
GSC-14900-1

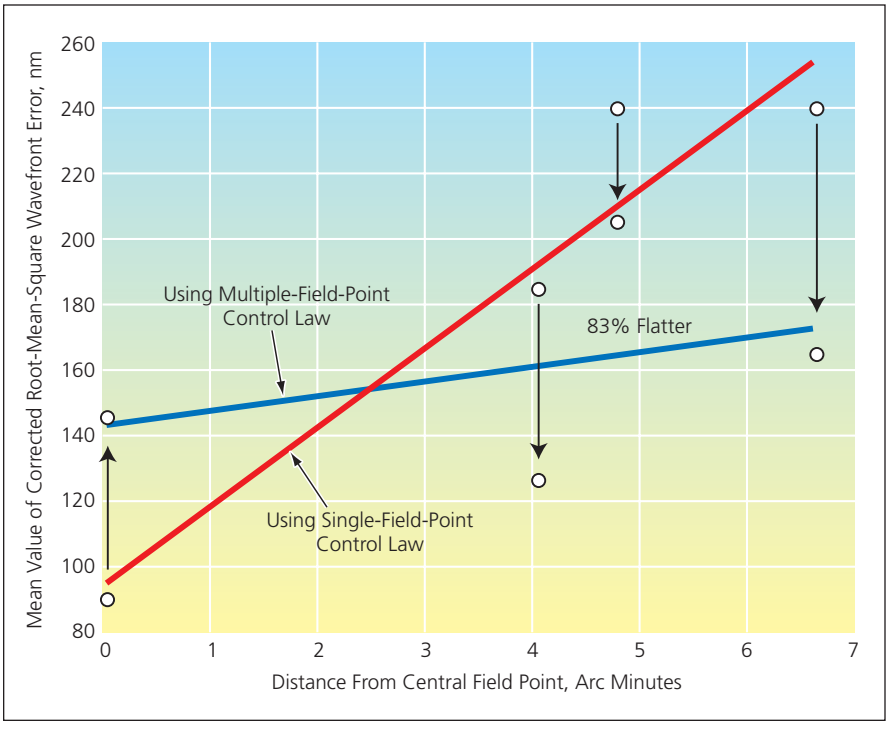

Mean Values of Corrected Root-Mean-Square Wavefront Error were computed for several field points and fitted with straight lines to show that errors can be reduced and/or distributed more evenly when multiple field points and the filter function are used.

Iterative-Transform Phase Retrieval Using Adaptive Diversity

High- and low-spatial-frequency contents are recovered with high dynamic range.

Goddard Space Flight Center, Greenbelt, Maryland

A phase-diverse iterative-transform phase-retrieval algorithm enables high-spatial-frequency, high-dynamic-range, image-based wavefront sensing. [The terms "phase-diverse," "phase retrieval," "image-based," and "wavefront sensing" are defined in the first of the two immediately preceding articles, "Broadband Phase Retrieval for Image-Based Wavefront Sensing" (GSC-14899-1).] As described below, no prior phase-retrieval algorithm has offered both high dynamic range and the capability to recover high-spatial-frequency components.

Each of the previously developed image-based phase-retrieval techniques can be classified into one of two categories: iterative transform or parametric. Among the modifications of the original iterative-transform approach has been the introduction of a defocus diversity function (also defined in the cited companion article). Modifications of the original parametric approach have included minimizing alternative objective functions as well as implementing a variety of nonlinear optimization methods. The iterative-transform approach offers the advantage of ability to recover low, middle, and high spatial frequencies, but has disadvantage of having a limited dynamic range to one wavelength or less. In contrast, parametric phase retrieval offers the advantage of high dynamic range, but is poorly suited for recovering higher spatial frequency aberrations.

The present phase-diverse iterative-transform phase-retrieval algorithm offers both the high-spatial-frequency capability of the iterative-transform approach and the high dynamic range of parametric phase-recovery techniques. In implementation, this is a focus-diverse iterative-transform phase-retrieval algorithm that incorporates an adaptive diversity function, which makes it possible to avoid phase unwrapping while preserving high-spatial-frequency recovery.

The algorithm includes an inner and an outer loop (see figure). An initial estimate of phase is used to start the algorithm on the inner loop, wherein multiple intensity images are processed, each using a different defocus value. The processing is done by an iterative-transform method, yielding individual phase estimates corresponding to each image of the defocus-diversity data set. These individual phase estimates are combined in a weighted average to form a new phase estimate, which serves as the initial phase estimate for either the next iteration of the iterative-transform method or, if the maximum number of iterations has been reached, for the next

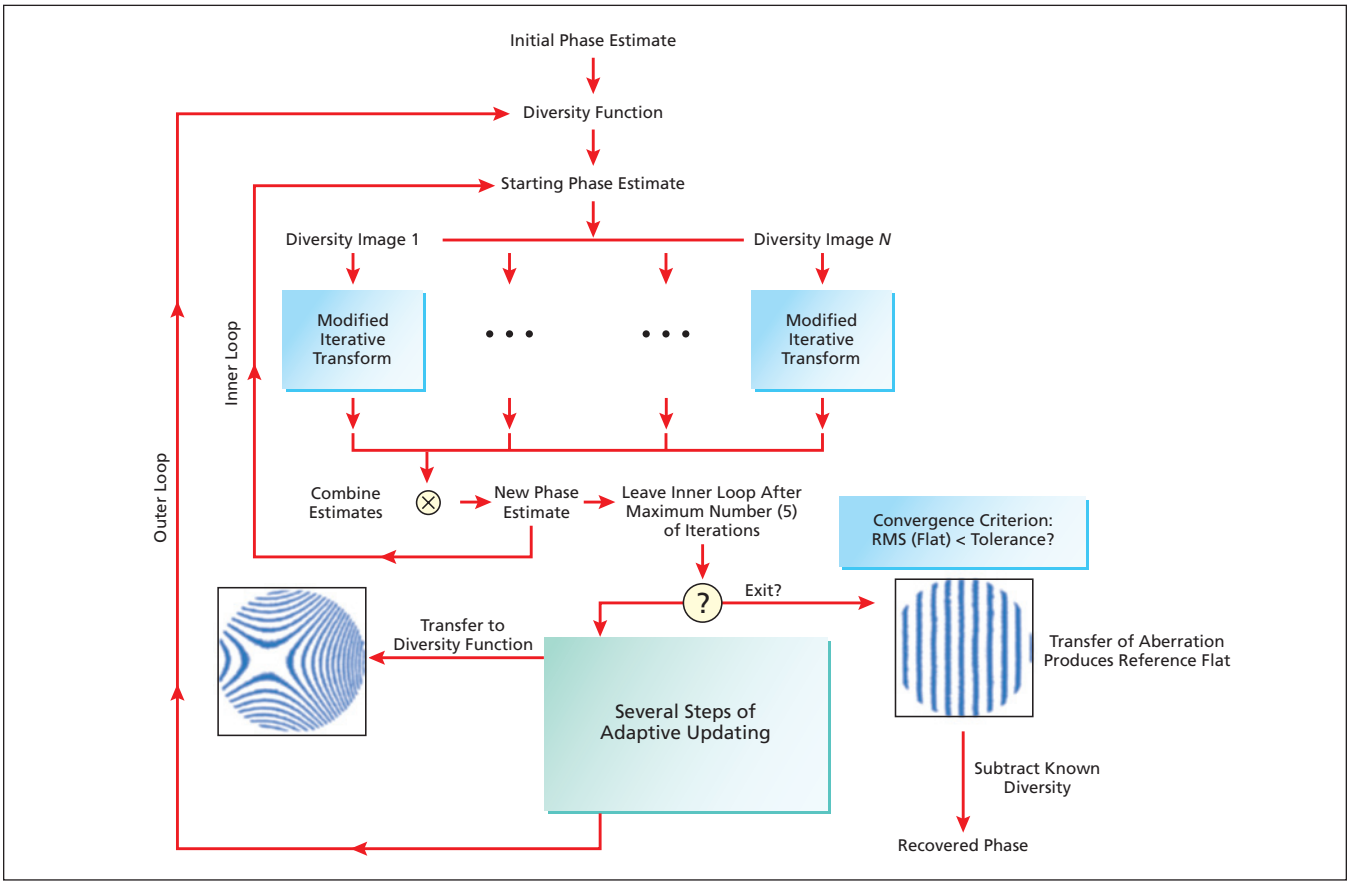

This **Phase-Diverse Iterative-Transform Phase-Retrieval Algorithm** incorporates an adaptive diversity function, which acts as feedback that makes it possible to avoid phase unwrapping while preserving high-spatial-frequency recovery.

several steps, which constitute the outer-loop portion of the algorithm.

The details of the next several steps must be omitted here for the sake of brevity. The overall effect of these steps is to adaptively update the diversity defocus values according to recovery of global defocus in the phase estimate. Aberration recovery varies with differing amounts as the amount of diversity defocus is updated in each image; thus, feedback is incorporated into the recovery process. This process is iterated until the global defocus error is driven to zero during the recovery process.

The amplitude of aberration may far exceed one wavelength after completion of the inner-loop portion of the algorithm, and the classical iterative transform method does not, by itself, enable recovery of multi-wavelength aberrations. Hence, in the absence of a means of "off-loading" the multi-wavelength portion of the aberration, the algorithm would produce a wrapped phase map. However, a special aberration-fitting procedure can be applied to the wrapped phase data to transfer at least some portion of the multi-wavelength aberration to the diversity function, wherein the data are treated as known phase values. In this way, a multi-wavelength aberration can be recovered incrementally by successively applying the aberration-fitting procedure to intermediate wrapped phase maps. During recovery, as more of the aberration is transferred to the diversity function following successive iterations around the outer loop, the estimated phase ceases to wrap in places where the aberration values become incorporated as part of the diversity function. As a result, as the aberration content is transferred to the diversity function, the phase estimate resembles that of a reference flat.

This work was done by Bruce H. Dean of Goddard Space Flight Center. Further information is contained in a TSP (see page 1).
GSC-14879-1

Wavefront Sensing With Switched Lenses for Defocus Diversity

It is no longer necessary to translate a camera to precisely controlled defocus positions.

Goddard Space Flight Center, Greenbelt, Maryland

In an alternative hardware design for an apparatus used in image-based wavefront sensing, defocus diversity is introduced by means of fixed lenses that are mounted in a filter wheel (see figure) so that they can be alternately switched into a position in front of the focal plane of an electronic camera recording the image formed by the optical system under test. [The terms "image-based", "wavefront sensing", and "defocus diversity" are defined in the first of the three immediately

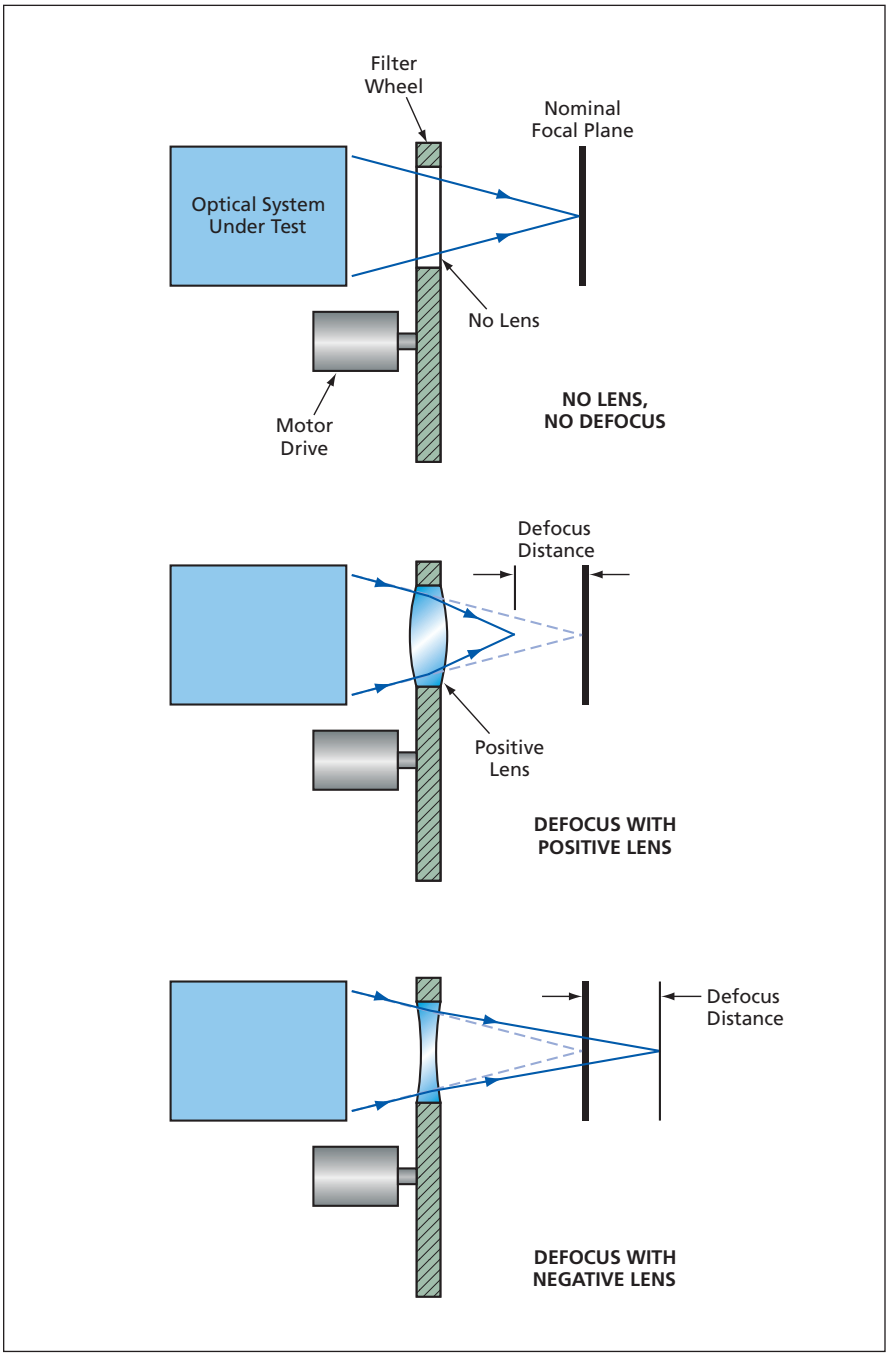

A **Known Amount of Defocus** is introduced by rotating the filter wheel to place a known positive or negative lens in front of the focal plane.

preceding articles, "Broadband Phase Retrieval for Image-Based Wavefront Sensing" (GSC-14899-1).] Each lens in the filter wheel is designed so that the optical effect of placing it at the assigned position is equivalent to the optical effect of translating the camera a specified defocus distance along the optical axis.

Heretofore, defocus diversity has been obtained by translating the imaging camera along the optical axis to various defocus positions. Because data must be taken at multiple, accurately measured defocus positions, it is necessary to mount the camera on a precise translation stage that must be calibrated for each defocus position and/or to use an optical encoder for measurement and feedback control of the defocus positions. Additional latency is introduced into the wavefront-sensing process as the camera is translated to the various defocus positions. Moreover, if the optical system under test has a large focal length, the required defocus values are large, making it necessary to use a correspondingly bulky translation stage.

By eliminating the need for translation of the camera, the alternative design simplifies and accelerates the wavefront-sensing process. This design is cost-effective in that the filter-wheel/lens mechanism can be built from commercial catalog components. After initial calibration of the defocus value of each lens, a selected defocus value is introduced by simply rotating the filter wheel to place the corresponding lens in front of the camera. The rotation of the wheel can be automated by use of a motor drive, and further calibration is not necessary. Because a camera-translation stage is no longer needed, the size of the overall apparatus can be correspondingly reduced.

This work was done by Bruce H. Dean of Goddard Space Flight Center. Further information is contained in a TSP (see page 1).
GSC-14901-1

Smooth Phase Interpolated Keying

Excellent performance can be obtained without excessive complexity.

Goddard Space Flight Center, Greenbelt, Maryland

Smooth phase interpolated keying (SPIK) is an improved method of computing smooth phase-modulation waveforms for radio communication systems that convey digital information. SPIK is applicable to a variety of phase-shift-keying (PSK) modulation schemes, including quaternary PSK (QPSK), octonary PSK (8PSK), and 16PSK. In comparison with a related prior method, SPIK offers advantages of better performance and less complexity of implementation.

In a PSK scheme, the underlying information waveform that one seeks to convey consists of discrete rectangular steps, but the spectral width of such a waveform is excessive for practical radio communication. Therefore, the problem is to smooth the step phase waveform in such a manner as to maintain power and bandwidth efficiency without incurring an unacceptably large error rate and without introducing undesired variations in the amplitude of the affected radio signal. Although the ideal constellation of PSK phasor points does not cause amplitude variations, filtering of the modulation waveform (in which, typically, a rectangular pulse is converted to a square-root raised cosine pulse) causes amplitude fluctuations. If a power-efficient nonlinear amplifier is used in the radio communication system, the fluctuating-amplitude signal can undergo significant spectral regrowth, thus compromising the bandwidth efficiency of the system.

In the related prior method, one seeks to solve the problem in a procedure that comprises two major steps: phase-value generation and phase interpolation. SPIK follows the two-step approach of the related prior method, but the details of the steps are different. In the phase-value-generation step, the phase values of symbols in the PSK constellation are determined by a phase function that is said to be maximally smooth and that is chosen to minimize the spectral spread of the modulated signal. In this step, the constellation is divided into two groups by assigning, to information symbols, phase values that result in equal numbers of clockwise and counter-clockwise phase rotations for equally likely symbols. The purpose served by assigning phase values in this way is to prevent unnecessary generation of spectral lines and prevent net shifts of the carrier signal. In the phase-interpolation step, the smooth phase values are interpolated over a number, n, of consecutive symbols (including the present symbol) by means of an unconventional spline curve fit.

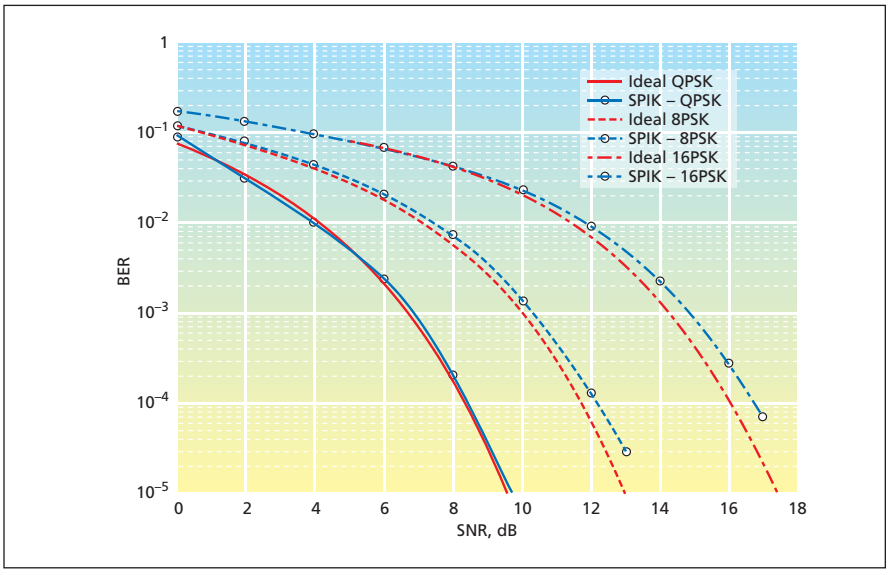

The **BER Performances** achievable in three PSK modulation schemes with SPIK were found to be only slightly worse than the corresponding ideal BER performances.

SPIK offers several advantages over the prior method:

- SPIK is not subject to numerical overflow that can occur because of phase buildup in the prior method.
- SPIK does not result in the unwanted spectral lines that are generated when the prior method is applied to QPSK.
- Whereas n can vary (and, hence, the phase of the present symbol can vary accordingly) in the prior method, n is fixed (typically at 3) in the present method.
- SPIK is amenable to simpler, optimal receiver structures.

It should be noted that the interpolator length (n) is an important parameter in SPIK. The reasons favoring the choice of $n = 3$ are

- Both the transmitter and the receiver can be implemented in architectures of low complexity;
- Performance at $n = 3$ is noticeably better than that at $n = 2$; and
- Performance for all values of $n>3$ is only slightly better than that for $n = 3$.

Computational simulations have been performed to evaluate the bit-error rate (BER) as a function of signal-to-noise ratio (SNR) for ideal QPSK, 8-PSK, and 16-PSK, and for the corresponding PSK cases with SPIK. The results, plotted in the figure, show that performance attainable with SPIK is close to ideal. In addition, the spectral and BER performances of SPIK-QPSK have been shown to exceed those of enhanced Feher QPSK.

This work was done by Deva K. Borah of New Mexico State University for Goddard Space Flight Center.

In accordance with Public Law 96-517, the contractor has elected to retain title to this invention. Inquiries concerning rights for its commercial use should be addressed to:

New Mexico State University
P.O. Box 30001
MSC 3RES
Las Cruces, NM 88003-8001

Refer to GSC-14882-1, volume and number of this NASA Tech Briefs *issue, and the page number.*

Maintaining Stability During a Conducted-Ripple EMC Test

Ripple is now injected via amplifier-controlled FETs instead of a transformer.

NASA's Jet Propulsion Laboratory, Pasadena, California

An improved technique, and electronic circuitry to implement the technique, have been developed for a military-standard electromagnetic-compatibility (EMC) test in which one analyzes susceptibility to low-frequency ripple conducted into the equipment under test via a DC power line. In the traditional technique for performing the particular test, the ripple is coupled onto the DC power line via a transformer. Depending upon some design details of the equipment under test, the inductance of the transformer can contribute a degree of instability that results in an oscillation of amplitude large enough to destroy the equipment.

It is usually possible to suppress the oscillation by connecting a damping resistor to the primary terminals of the ripple-injection transformer. However, it is important to emphasize the "usually" in the preceding sentence: sometimes, the resistive damping becomes insufficient to suppress destructive oscillation. In addition, undesirably, the resistor contributes to power dissipation and power demand, and thereby also necessitates the use of a larger ripple-voltage amplifier. Yet another disadvantage of the transformer-coupling technique is that the transformer introduces low-frequency distortion of the injected ripple voltage.

The improved technique makes it possible to inject ripple with very low distortion at low frequency, without inducing oscillation. In this technique, a transformer is not used: Instead, power is fed to the equipment under test via series power field-effect transistors (FETs) controlled by a summing operational amplifier. One of the inputs to the amplifier controls the DC component of the power-line voltage; the other input, generated by an external oscillator, controls the ripple component. The circuitry for implementing this technique includes panel displays, an internal power supply for the operational amplifier and panel displays, and amplitude controls for the DC and ripple power-line voltage components.

This work was done by Vatche Vorperian of Caltech for NASA's Jet Propulsion Laboratory. Further information is contained in a TSP (see page 1). NPO-30652

Photodiode Preamplifier for Laser Ranging With Weak Signals

This circuit suppresses noise without sacrificing timing accuracy.

NASA's Jet Propulsion Laboratory, Pasadena, California

An improved preamplifier circuit has been designed for processing the output of an avalanche photodiode (APD) that is used in a high-resolution laser ranging system to detect laser pulses returning from a target. The improved circuit stands in contrast to prior such circuits in which the APD output current pulses are made to pass, variously, through wide-band or narrow-band load networks before preamplification. A major disadvantage of the prior wide-band load networks is that they are highly susceptible to noise, which degrades timing resolution. A major disadvantage of the prior narrow-band load networks is that they make it difficult to sample the amplitudes of the narrow laser pulses ordinarily used in ranging.

In the improved circuit, a load resistor is connected to the APD output and its value is chosen so that the time constant defined by this resistance and the APD capacitance is large, relative to the duration of a laser pulse. The APD capacitance becomes initially charged by the pulse of current generated by a return laser pulse, so that the rise time of the load-network output is comparable to the duration of the return pulse. Thus, the load-network output is characterized by a fast-rising leading edge, which is necessary for accurate pulse timing.

On the other hand, the resistance-capacitance combination constitutes a low-pass filter, which helps to suppress noise. The long time constant causes the load-network output pulse to have a long shallow-sloping trailing edge, which makes it easy to sample the amplitude of the return pulse. The output of the load network is fed to a low-noise, wide-band amplifier. The amplifier must be a wide-band one in order to preserve the sharp pulse rise for timing. The suppression of noise and the use of a low-noise amplifier enable the ranging system to detect relatively weak return pulses.

This work was done by Alexander Abramovici and Jacob Chapsky of Caltech for NASA's Jet Propulsion Laboratory. Further information is contained in a TSP (see page 1).
NPO-30598

Advanced High-Definition Video Cameras

Marshall Space Flight Center, Alabama

A product line of high-definition color video cameras, now under development, offers a superior combination of desirable characteristics, including high frame rates, high resolutions, low power consumption, and compactness. Several of the cameras feature a 3,840 × 2,160-pixel format with progressive scanning at 30 frames per second. The power consumption of one of these cameras is about 25 W. The size of the camera, excluding the lens assembly, is 2 by 5 by 7 in. (about 5.1 by 12.7 by 17.8 cm).

The aforementioned desirable characteristics are attained at relatively low

cost, largely by utilizing digital processing in advanced field-programmable gate arrays (FPGAs) to perform all of the many functions (for example, color-balance and contrast adjustments) of a professional color video camera. The processing is programmed in VHDL so that application-specific integrated circuits (ASICs) can be fabricated directly from the program. ["VHDL" signifies VHSIC Hardware Description Language C, a computing language used by the United States Department of Defense for describing, designing, and simulating very-high-speed integrated circuits (VHSICs).]

The image-sensor and FPGA clock frequencies in these cameras have generally been much higher than those used in video cameras designed and manufactured elsewhere. Frequently, the outputs of these cameras are converted to other video-camera formats by use of pre- and post-filters.

This work was done by William Glenn of Florida Atlantic University for Marshall Space Flight Center. For further information, contact Jerry Engelbrecht at 561-297-2335. MFS-32091-1

Circuit for Full Charging of Series Lithium-Ion Cells

Differences among cells would no longer prevent full charging.

Lyndon B. Johnson Space Center, Houston, Texas

An advanced charger has been proposed for a battery that comprises several lithium-ion cells in series. The proposal is directed toward charging the cells in as nearly an optimum manner as possible despite unit-to-unit differences among the nominally identical cells.

The particular aspect of the charging problem that motivated the proposal can be summarized as follows: During bulk charging (charging all the cells in series at the same current), the voltages of individual cells increase at different rates. Once one of the cells reaches full charge, bulk charging must be stopped, leaving other cells less than fully charged.

To make it possible to bring all cells up to full charge once bulk charging has been completed, the proposed charger would include a number of "top-off" chargers — one for each cell. The top-off chargers would all be powered from the same DC source, but their outputs would be DC-isolated from each other and AC-coupled to their respective cells by means of transformers, as described below.

Each top-off charger would include a flyback transformer, an electronic switch, and an output diode. For suppression of undesired electromagnetic emissions, each top-off charger would also include (1) a resistor and capacitor configured to act as a snubber and (2) an inductor and capacitor configured as a filter. The magnetic characteristics of the flyback transformer and the duration of its output pulses determine the energy delivered to the lithium-ion cell.

It would be necessary to equip the cell with a precise voltage monitor to determine when the cell reaches full charge. In response to a full-charge reading by this voltage monitor, the electronic switch would be held in the "off" state. Other cells would continue to be charged similarly by their top-off chargers until their voltage monitors read full charge.

This work was done by William E. Ott and David L. Saunders of Honeywell, Inc. for Johnson Space Center.

Title to this invention has been waived under the provisions of the National Aeronautics and Space Act {42 U.S.C. 2457(f)}, to Honeywell, Inc. Inquiries concerning licenses for its commercial development should be addressed to:

Honeywell, Inc.
P.O. Box 52199
Phoenix, AZ 85072-2199

Refer to MSC-23503, volume and number of this NASA Tech Briefs *issue, and the page number.*

Analog Nonvolatile Computer Memory Circuits

Digital data would be stored in analog form in FFETs.

Marshall Space Flight Center, Alabama

In nonvolatile random-access memory (RAM) circuits of a proposed type, digital data would be stored in analog form in ferroelectric field-effect transistors (FFETs). This type of memory circuit would offer advantages over prior volatile and nonvolatile types:

- In a conventional complementary metal oxide/semiconductor static RAM, six transistors must be used to store one bit, and storage is volatile in that data are lost when power is turned off. In a conventional dynamic RAM, three transistors must be used to store one bit, and the stored bit must be refreshed every few milliseconds. In contrast, in a RAM according to the proposal, data would be retained when power was turned off, each memory cell would contain only two FFETs, and the cell could store multiple bits (the exact number of bits depending on the specific design).
- Conventional flash memory circuits afford nonvolatile storage, but they operate at reading and writing times of the order of thousands of conventional computer memory reading and writing times and, hence, are suitable for use only as off-line storage devices. In addition, flash memories cease to function after limited numbers of writing cycles. The proposed memory circuits would not be subject to either of these limitations.
- Prior developmental nonvolatile ferroelectric memories are limited to one bit per cell, whereas, as stated above, the proposed memories would not be so limited.

The design of a memory circuit according to the proposal must reflect the fact that FFET storage is only partly nonvolatile, in that the signal stored in an FFET decays gradually over time. (Retention times of some advanced FFETs exceed

ten years.) Instead of storing a single bit of data as either a positively or negatively saturated state in a ferroelectric device, each memory cell according to the proposal would store two values. The two FFETs in each cell would be denoted the storage FFET and the control FFET. The storage FFET would store an analog signal value, between the positive and negative FFET saturation values. This signal value would represent a numerical value of interest corresponding to multiple bits: for example, if the memory circuit were designed to distinguish among 16 different analog values, then each cell could store 4 bits. Simultaneously with writing the signal value in the storage FFET, a negative saturation signal value would be stored in the control FFET. The decay of this control-FFET signal from the saturation value would serve as a model of the decay, for use in regenerating the numerical value of interest from its decaying analog signal value.

The memory circuit would include addressing, reading, and writing circuitry that would have features in common with the corresponding parts of other memory circuits, but would also have several distinctive features. The writing circuitry would include a digital-to-analog converter (DAC); the reading circuitry would include an analog-to-digital converter (ADC). For writing a numerical value of interest in a given cell, that cell would be addressed, the saturation value would be written in the control FFET in that cell, and the non-saturation analog value representing the numerical value of interest would be generated by use of the DAC and stored in the storage FFET in that cell. For reading the numerical value of interest stored in a given cell, the cell would be addressed, the ADC would convert the decaying control and storage analog signal values to digital values, and an associated fast digital processing circuit would regenerate the numerical value from digital values.

This work was done by Todd MacLeod of Marshall Space Flight Center. Further information is contained in a TSP (see page 1).

This invention is owned by NASA, and a patent application has been filed. For further information, contact Sammy Nabors, MSFC Commercialization Assistance Lead, at sammy.a.nabors@nasa.gov. Refer to MFS-32208-1.

JavaGenes Molecular Evolution

JavaGenes is a general-purpose, evolutionary software system written in Java. It implements several versions of a genetic algorithm, simulated annealing, stochastic hill climbing, and other search techniques. This software has been used to evolve molecules, atomic force field parameters, digital circuits, Earth Observing Satellite schedules, and antennas. This version differs from version 0.7.28 in that it includes the molecule evolution code and other improvements. Except for the antenna code, JaveGenes is available for NASA Open Source distribution.

This program was written by Jason Lohn, David Smith, and Jeremy Frank of Ames Research Center; Al Globus of Computer Science Corp.; and James Crawford of Universities Space Research Association. For further information, access http://opensource.arc.nasa.gov or contact the Ames Technology Partnerships Division at (650) 604-2954. ARC-15103-1

World Wind 3D Earth Viewing

World Wind allows users to zoom from satellite altitude down to any place on Earth, leveraging high-resolution LandSat imagery and SRTM (Shuttle Radar Topography Mission) elevation data to experience Earth in visually rich 3D. In addition to Earth, World Wind can also visualize other planets, and there are already comprehensive data sets for Mars and the Earth's moon, which are as easily accessible as those of Earth.

There have been more than 20 million downloads to date, and the software is being used heavily by the Department of Defense due to the code's ability to be extended and the evolution of the code courtesy of NASA and the user community. Primary features include the dynamic access to public domain imagery and its ease of use. All one needs to control World Wind is a two-button mouse. Additional guides and features can be accessed through a simplified menu. A JAVA version will be available soon. Navigation is automated with single clicks of a mouse, or by typing in any location to automatically zoom in to see it.

The World Wind install package contains the necessary requirements such as the .NET runtime and managed DirectX library. World Wind can display combinations of data from a variety of sources, including Blue Marble, LandSat 7, SRTM, NASA Scientific Visualization Studio, GLOBE, and much more. A thorough list of features, the user manual, a key chart, and screen shots are available at http://worldwind.arc.nasa.gov.

This program was written by Patrick Hogan of Ames Research Center, Christopher Maxwell and Randolph Kim of National Space Grant Foundation, and Tom Gaskins. For further information, access http://worldwind.arc.nasa.gov/ or contact the Ames Technology Partnerships Division at (650) 604-2954. ARC-15166-1.

Lithium Dinitramide as an Additive in Lithium Power Cells

This inorganic additive appears to act as a superior SEI promoter.

John H. Glenn Research Center, Cleveland, Ohio

Lithium dinitramide, $LiN(NO_2)_2$ has shown promise as an additive to non-aqueous electrolytes in rechargeable and non-rechargeable lithium-ion-based electrochemical power cells. Such non-aqueous electrolytes consist of lithium salts dissolved in mixtures of organic ethers, esters, carbonates, or acetals. The benefits of adding lithium dinitramide (which is also a lithium salt) include lower irreversible loss of capacity on the first charge/discharge cycle, higher cycle life, lower self-discharge, greater flexibility in selection of electrolyte solvents, and greater charge capacity.

The need for a suitable electrolyte additive arises as follows: The metallic lithium in the anode of a lithium-ion-based power cell is so highly reactive that in addition to the desired main electrochemical reaction, it engages in side reactions that cause formation of resistive films and dendrites, which degrade performance as quantified in terms of charge capacity, cycle life, shelf life, first-cycle irreversible capacity loss, specific power, and specific energy. The incidence of side reactions can be reduced through the formation of a solid-electrolyte interface (SEI) — a thin film that prevents direct contact between the lithium anode material and the electrolyte. Ideally, an SEI should chemically protect the anode and the electrolyte from each other while exhibiting high conductivity for lithium ions and little or no conductivity for electrons. A suitable additive can act as an SEI promoter.

Heretofore, most SEI promotion was thought to derive from organic molecules in electrolyte solutions. In contrast, lithium dinitramide is inorganic. Dinitramide compounds are known as oxidizers in rocket-fuel chemistry and until now, were not known as SEI promoters in battery chemistry. Although the exact reason for the improvement afforded by the addition of lithium dinitramide is not clear, it has been hypothesized that lithium dinitramide competes with other electrolyte constituents to react with lithium on the surface of the anode to form a beneficial SEI. Apparently, nitrides and oxides that result from reduction of lithium dinitramide on the anode produce a thin, robust SEI different from the SEIs formed from organic SEI promoters. The SEI formed from lithium dinitramide is more electronically insulating than is the film formed in the presence of an otherwise identical electrolyte that does not include lithium dinitramide. SEI promotion with lithium dinitramide is useful in batteries with metallic lithium and lithium alloy anodes.

This work was done by Alexander A. Gorkovenko of Material Methods LLC for Glenn Research Center.

Inquiries concerning rights for the commercial use of this invention should be addressed to NASA Glenn Research Center, Innovative Partnerships Office, Attn: Steve Fedor, Mail Stop 4–8, 21000 Brookpark Road, Cleveland, Ohio 44135. Refer to LEW-17983-1.

Accounting for Uncertainties in Strengths of SiC MEMS Parts

Fracture strength of a part can be predicted as one statistical distribution.

John H. Glenn Research Center, Cleveland, Ohio

A methodology has been devised for accounting for uncertainties in the strengths of silicon carbide structural components of microelectromechanical systems (MEMS). The methodology enables prediction of the probabilistic strengths of complexly shaped MEMS parts using data from tests of simple specimens. This methodology is intended to serve as a part of a rational basis for designing SiC MEMS, supplementing methodologies that have been borrowed from the art of designing macroscopic brittle material structures.

The need for this or a similar methodology arises as a consequence of the fundamental nature of MEMS and the brittle silicon-based materials of which they are typically fabricated. When tested to fracture, MEMS and structural components thereof show wide part-to-part scatter in strength. The methodology involves the use of the Ceramics Analysis and Reliability Evaluation of Structures Life (CARES/Life) software in conjunction with the ANSYS Probabilistic Design System (PDS) software to simulate or predict the strength responses of brittle material components while simultaneously accounting for the effects of variability of geometrical features on the strength responses. As such, the methodology involves the use of an extended version of the ANSYS/CARES/PDS software system described in "Probabilistic Prediction of Lifetimes of Ceramic Parts" (LEW-17682-1/4-1), *Software Tech Briefs* supplement to *NASA Tech Briefs*, Vol. 30, No. 9 (September 2006), page 10.

The ANSYS PDS software enables the ANSYS finite-element-analysis program to account for uncertainty in the design-and-analysis process. The ANSYS PDS software accounts for uncertainty in material properties, dimensions, and loading by assigning probabilistic distributions to user-specified model parameters and performing simulations using various sampling techniques. The CARES/Life code predicts the time-dependent probabilities of failure of brittle material structures under thermomechanical loads.

In the present methodology, CARES/Life is used with ANSYS/PDS to simulate the effect of variations of dimensions on the predicted probabilities of failure of SiC specimens. A special ANSYS macroinstruction code was developed for this pur-

pose. This macroinstruction code simulates fracture strengths of specimens by use of a combination of a random-number generator (for probability of failure), CARES/Life, and ANSYS finite-element modeling for specimens having randomly chosen dimensions based on a statistical distribution and parameters thereof specified by the user. A unique contribution of this macroinstruction code is that given multiple stochastic input variables, including those pertaining to the strength of the material and the geometry of the part, one can now predict the fracture strength of a complexly shaped part as a single statistical distribution, and can predict a single value of probability of failure for a given load. This capability makes it possible to directly compare predictions made by use of CARES/Life with data from tests of specimens while accounting for the significant amounts of variability that are common in dimensions of MEMS structures.

The methodology was tested by applying it to submillimeter-sized single-crystal SiC tensile specimens fabricated by deep reactive-ion etching. The specimens had large thickness-to-width ratios (high-aspect-ratios). Some of the specimens contained, variously, elliptical or circular through-thickness holes, which served as stress concentrators. The roughness of the sidewalls left by etching was greater than that of the top and bottom specimen surfaces. There was a large amount of scatter in the measured fracture strengths (typical for ceramics), but the average fracture strength was observed to increase with greater concentration of stress. Variations in dimensions among specimens were measured. The aforementioned macroinstruction code was used to predict the fracture strengths of the specimens with the stress-concentrating holes and the variations in dimensions.

The predictions were found to correlate well with data from tests of the specimens containing circular holes but not quite as well with data from tests of the specimens containing elliptical holes. The results were interpreted as signifying, in part, that (1) the Weibull distribution, which is used in the CARES/Life software, adequately characterizes the distribution of strengths of MEMS parts; (2) the surface areas of the relatively rough etched sidewalls likely controlled the observed failure responses; (3) the methodology enables accounting for part-to-part variations in dimensions and other properties; and (4) at least at moderate levels of concentration of stress, the methodology can be used to enable successful design of complexly shaped parts on the basis of data from tests of simply shaped specimens.

This work was done by Noel Nemeth, Laura Evans, Glen Beheim, and Mark Trapp of Glenn Research Center; Osama Jadaan of the University of Wisconsin; and William N. Sharpe, Jr., of Johns Hopkins University. Further information is contained in a TSP (see page 1).

Inquiries concerning rights for the commercial use of this invention should be addressed to NASA Glenn Research Center, Innovative Partnerships Office, Attn: Steve Fedor, Mail Stop 4–8, 21000 Brookpark Road, Cleveland, Ohio 44135. Refer to LEW-18095-1.

Ion-Conducting Organic/Inorganic Polymers

Properties can be tailored through a choice of starting alkoxysilane and diamine ingredients.

John H. Glenn Research Center, Cleveland, Ohio

Ion-conducting polymers that are hybrids of organic and inorganic moieties and that are suitable for forming into solid-electrolyte membranes have been invented in an effort to improve upon the polymeric materials that have been used previously for such membranes. Examples of the prior materials include perfluorosulfonic acid-based formulations, polybenzimidazoles, sulfonated polyetherketone, sulfonated naphthalenic polyimides, and polyethylene oxide (PEO)-based formulations. Relative to the prior materials, the polymers of the present invention offer greater dimensional stability, greater ease of formation into mechanically resilient films, and acceptably high ionic conductivities over wider temperature ranges. Devices in which films made of these ion-conducting organic/inorganic polymers could be used include fuel cells, lithium batteries, chemical sensors, electrochemical capacitors, electrochromic windows and display devices, and analog memory devices.

The synthesis of a polymer of this type (see Figure 1) starts with a reaction between an epoxide-functionalized alkoxysilane and a diamine. The product of this reaction is polymerized by hydrolysis and condensation of the alkoxysilane group, producing a molecular network that contains both organic and inorganic (silica) links. The silica in the network contributes to the ionic conductivity and to the desired thermal and mechanical properties.

Examples of other diamines that have been used in the reaction sequence of Figure 1 are shown in Figure 2. One can

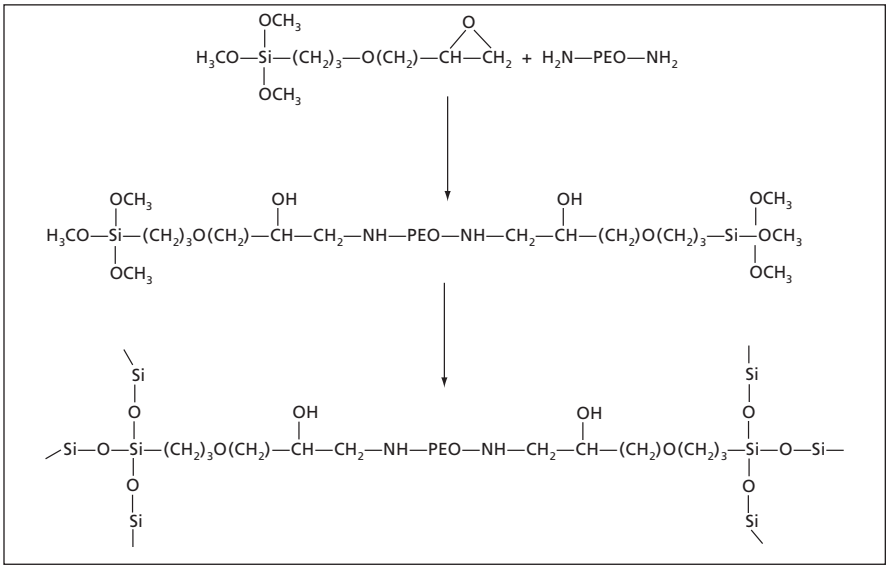

Figure 1. A **Molecular Network of Organic and Inorganic Moieties** is produced in this representative reaction sequence. The starting alkoxysilane and diamine can be other than the ones shown here.

use any of these diamines or any combination of them in proportions chosen to impart desired properties to the finished product. Alternatively or in addition, one could similarly vary the functionality of the alkoxysilane to obtain desired properties. The variety of available alkoxysilanes and diamines thus affords flexibility to optimize the organic/inorganic polymer for a given application.

This work was done by James D. Kinder and Mary Ann B. Meador of Glenn Research Center. Further information is contained in a TSP (see page 1).

Inquiries concerning rights for the commercial use of this invention should be addressed to NASA Glenn Research Center, Innovative Partnerships Office, Attn: Steve Fedor, Mail Stop 4–8, 21000 Brookpark Road, Cleveland, Ohio 44135. Refer to LEW-17592-1.

MoO_3 Cathodes for High-Temperature Lithium Thin-Film Cells

Cycle lives of these cathodes exceed those of $LiCoO_2$ and $LiMn_2O_4$ cathodes.

NASA's Jet Propulsion Laboratory, Pasadena, California

MoO_3 has shown promise as a cathode material that can extend the upper limit of operating temperature of rechargeable lithium thin-film electrochemical cells. Cells of this type are undergoing development for use as energy sources in cellular telephones, wireless medical sensors, and other, similarly sized portable electronic products. The $LiCoO_2$ and $LiMn_2O_4$ cathodes heretofore used in these cells exhibit outstanding cycle lives (of the order of hundreds of thousands of cycles) at room temperature, but operation at higher temperatures reduces their cycle lives substantially: for example, at a temperature of 150 °C, cells containing $LiCoO_2$ cathodes lose half their capacities in 100 charge/discharge cycles.

The superiority of MoO_3 as a cathode material was demonstrated in experiments on lithium thin-film cells fabricated on glass slides. Each cell included a layer of Ti (for adhesion to the glass slide), a patterned layer of Pt that served as a cathode current collector, a cathode layer of MoO_3, a solid electrolyte layer of $Li_{3.3}PO_{3.8}N_{0.22}$ ("LiPON"), and an anode layer of Li. All the layers were deposited by magnetron sputtering except for the Li layer, which was deposited by thermal evaporation.

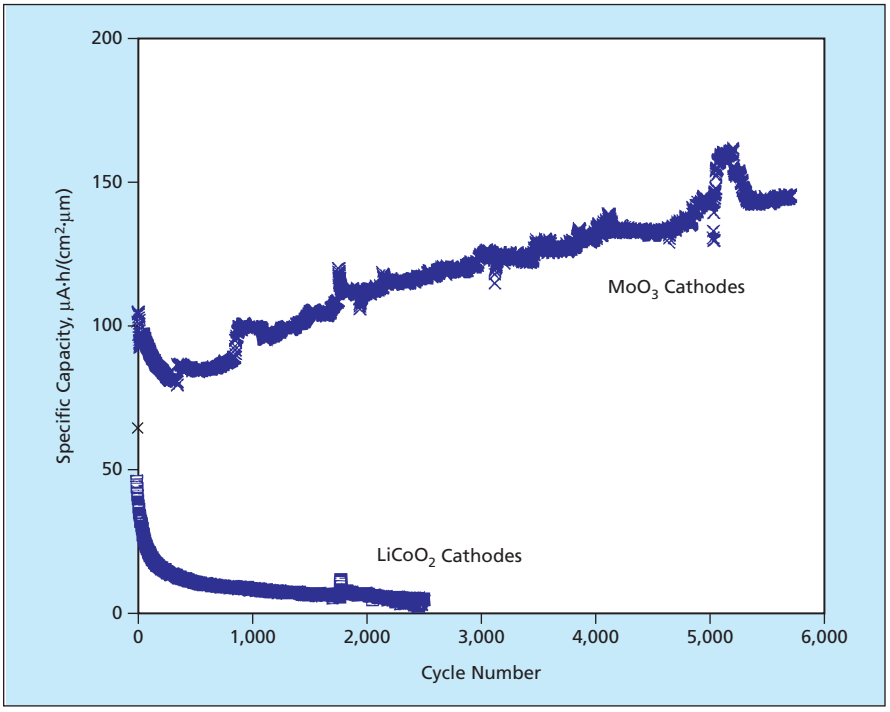

The **Specific Capacities and Cycle Lives** of cells containing $LiCoO_2$ and MoO_3 cathodes at a temperature of 150 °C were measured in charge/discharge cycling at a current density of 0.7 mA/cm^2.

These cells, along with similar ones containing $LiCoO_2$ cathodes, were subjected to several tests, including measurements of specific capacity in charge/discharge cycling at a temperature of 150 °C. The results of these measurements, plotted in the figure, showed that whereas specific capacity of the cells containing $LiCoO_2$ cathodes faded to about half its initial value after only 100 cycles, the specific capacity of the cells containing the MoO_3 cathodes faded only slightly during the first few hundred cycles and thereafter not only recovered to its initial value but continued to increase up to at least 5,500 cycles.

This work was done by William West and Jay Whitacre of Caltech for NASA's Jet Propulsion Laboratory. Further information is contained in a TSP (see page 1).

In accordance with Public Law 96-517, the contractor has elected to retain title to this invention. Inquiries concerning rights for its commercial use should be addressed to:

Innovative Technology Assets Management
JPL
Mail Stop 202-233
4800 Oak Grove Drive
Pasadena, CA 91109-8099
(818) 354-2240
E-mail: iaoffice@jpl.nasa.gov

Refer to NPO-41099, volume and number of this NASA Tech Briefs *issue, and the page number.*

Counterrotating-Shoulder Mechanism for Friction Stir Welding

The weights and costs of fixtures for holding workpieces could be reduced.

Marshall Space Flight Center, Alabama

A counterrotating-shoulder mechanism has been proposed as an alternative to the mechanism and fixtures used in conventional friction stir welding. The mechanism would internally react most or all of the forces and torques exerted on the workpiece, making it unnecessary to react the forces and torques through massive external fixtures.

In conventional friction stir welding, a rotating pin tool is inserted into, and moved along, a weld seam. As the pin tool moves, it stirs together material from the opposite sides of the seam to form the weld. A large axial "plunge" force must be exerted upon the workpiece through and by the pin tool and a shoulder attached above the pin tool in order to maintain the pressure necessary for the process. The workpiece is secured on top of an anvil, which supports the workpiece against the axial plunge force and against the torque exerted by the pin tool and shoulder. The anvil and associated fixtures must be made heavy (and, therefore, are expensive) to keep the workpiece stationary. In addition, workpiece geometries must be limited to those that can be accommodated by the fixtures.

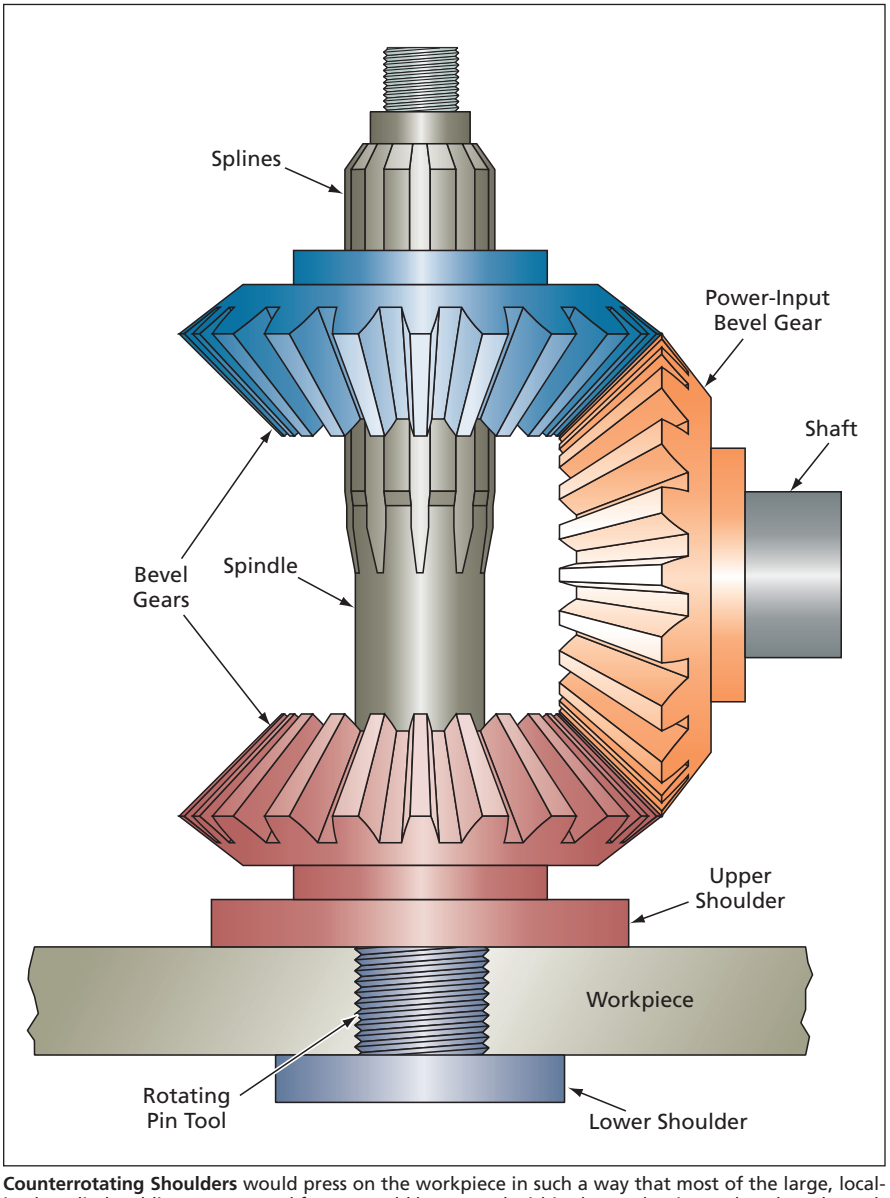

Counterrotating Shoulders would press on the workpiece in such a way that most of the large, localized applied welding torques and forces would be reacted within the mechanism rather than through external fixtures.

The predecessor of the proposed counterrotating-shoulder mechanism is a second-generation, "self-reacting" tool, resembling a bobbin, that makes it possible to dispense with the heavy anvil. This tool consists essentially of a rotating pin tool with opposing shoulders. Although the opposing shoulders maintain the necessary pressure without need to externally apply or react a large plunge force, the torque exerted on the workpiece remains unreacted in the absence of a substantial external fixture. Depending on the RPM and the thickness of the workpiece, the torque can be large.

The proposed mechanism (see figure) would include a spindle attached to a pin tool with a lower shoulder. The spindle would be coupled via splines to the upper one of three bevel gears in a differential drive. The middle bevel gear would be the power-input gear and would be coupled to the upper and lower bevel gears. The lower bevel gear would be attached to the upper shoulder and would slide and rotate freely over the spindle. The spindle would be fastened by its threaded upper end to an external submechanism that would exert axial tension on the spindle to load the workpiece in compression between the shoulders. By reducing or eliminating (relative to the use of a "self reacting" tool) the torque that must be reacted externally, the use of the proposed tool would reduce the tendency toward distortion or slippage of the workpiece.

To begin a weld, the spindle would be inserted through a hole in the workpiece or run-on tab at the beginning of the seam and fastened to the loading submechanism. Rotation and axial loading

would be increased gradually from zero and, after a time to be determined by trial and error, translation along the weld seam would be increased gradually from zero to a steady weld speed. The weld would be ended by running the mechanism off the workpiece or, if the lower shoulder were detachable, by detaching the lower shoulder from the spindle and pulling the pin tool out.

This work was done by Arthur C. Nunes, Jr., of Marshall Space Flight Center. Further information is contained in a TSP (see page 1).

This invention is owned by NASA, and a patent application has been filed. For further information, contact Sammy Nabors, MSFC Commercialization Assistance Lead, at sammy.a.nabors@nasa.gov. Refer to MFS-31648-1.

Strain Gauges Indicate Differential-CTE-Induced Failures

Failures are indicated by changes in slopes of strain versus temperature.

Goddard Space Flight Center, Greenbelt, Maryland

A method of detecting mechanical failure induced by variation in temperature at an adhesive bond between two materials that have different coefficients of thermal expansion (CTEs) involves monitoring of strain-gauge readings. This method can be regarded as an exploitation of the prior observation that the readings of strain gauges commonly used in tensile and compressive testing of material specimens include features indicative of incremental failures in the specimens. In this method, one or more strain gauges are bonded to either or both of the two materials near the bond between the materials. (The adhesive used to bond the strain gauges would not ordinarily be the same as the one used to bond the two materials). Then strain-gauge readings are recorded as the temperature of the materials is varied through a range of interest. Any significant discontinuity in the slope of the resulting strain-versus-temperature curve(s) is taken to be a qualitative indication of a failure of the bond between the two materials and/or a failure within one of the materials in the vicinity of the bond.

The method has been demonstrated in experiments on specimens consisting of polyacrylonitrile-fiber/epoxy-matrix laminated composite plates bonded by epoxy to smaller plates made, variously, of aluminum, titanium, and a low-CTE nickel/iron alloy. In preparation for each experiment, strain gauges were bonded, by use of cryogenic-rated adhesives, to the composite plate near the corners of the metal plate (see Figure 1). In each experiment, strain-gauge and temperature readings were taken as the specimen was cooled from room temperature to 20 K. The specimens were then returned to room temperature and ultrasonically inspected for damage in the bond region.

No failure events were detectable in the strain-gauge readings from the composite/titanium and composite/low-thermal-expansion-alloy specimens, and ultrasonic inspection of these specimens revealed no damage. However, failure events were seen in the strain-gauge readings from the composite/aluminum specimens (see Figure 2), and ultrasonic inspection confirmed that there was damage in the bond regions of these specimens.

This work was done by Brian Harris of Goddard Space Flight Center. Further information is contained in a TSP (see page 1). GSC-14984-1

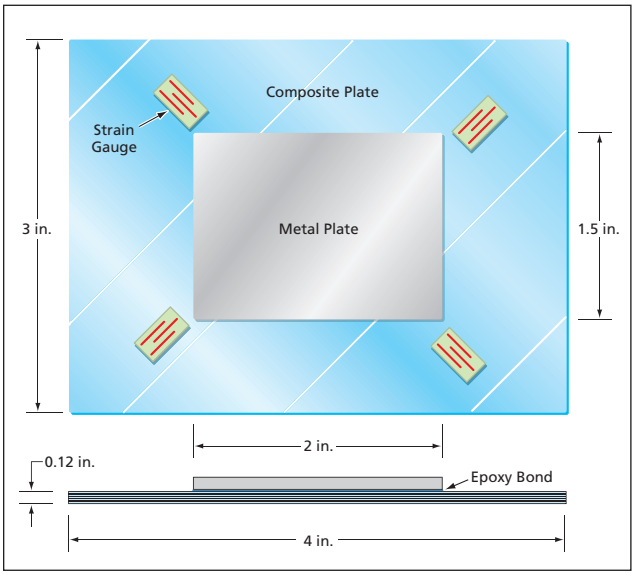

Figure 1. **Strain Gauges Were Bonded** to the composite plate near the corners of the metal plate because differential-thermal-expansion-induced stresses were expected to be large at these locations.

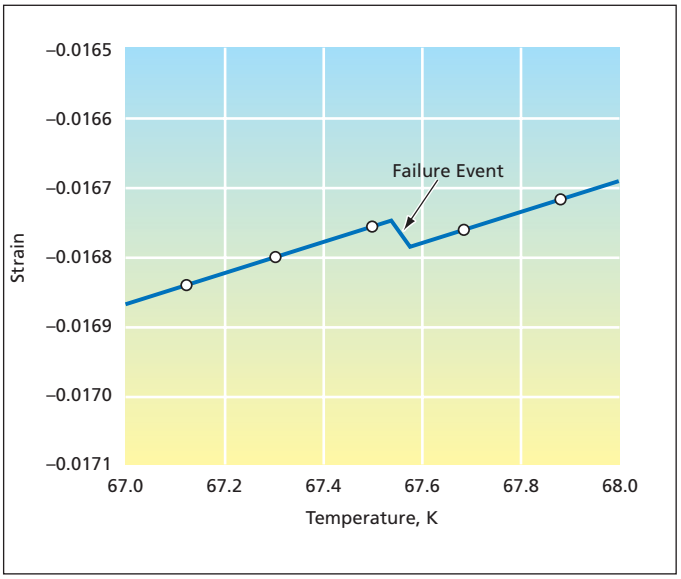

Figure 2. **Part of the Strain-Versus Temperature Curve** from one specimen includes a slope discontinuity indicative of a failure in the metal/composite bond region.

Antibodies Against Three Forms of Urokinase

These antibodies can be used to measure small quantities of three molecular forms of urokinase.

Lyndon B. Johnson Space Center, Houston, Texas

Antibodies that bind to preselected regions of the urokinase molecule have been developed. These antibodies can be used to measure small quantities of each of three molecular forms of urokinase that could be contained in microsamples or conditioned media harvested from cultures of mammalian cells. Previously available antibodies and assay techniques do not yield both clear distinctions among, and measurements of, all three forms.

Urokinase is a zymogen that is synthesized in a single-chain form, called "ScuPA," which is composed of 411 amino acid residues (see figure). ScuPA has very little enzyme activity, but it can be activated in two ways: (1) by cleavage of the peptide bond lysine 158/isoleucine 159 and the loss of lysine 158 to obtain the high molecular-weight (HMW) form of the enzyme or (2) by cleavage of the bond lysine 135/lysine 136 to obtain the low-molecular-weight (LMW) form of the enzyme.

The antibodies in question were produced in mice and rabbits by use of peptides as immunogens. The peptides were selected to obtain antibodies that bind to regions of ScuPA that include the lysine 158/isoleucine 159 and the lysine 135/lysine 136 bonds. The antibodies include monoclonal and polyclonal ones that yield indications as to whether either of these bonds is intact. The polyclonal antibodies include ones that preferentially bind to the HMW or LMW forms of the urokinase molecule. The

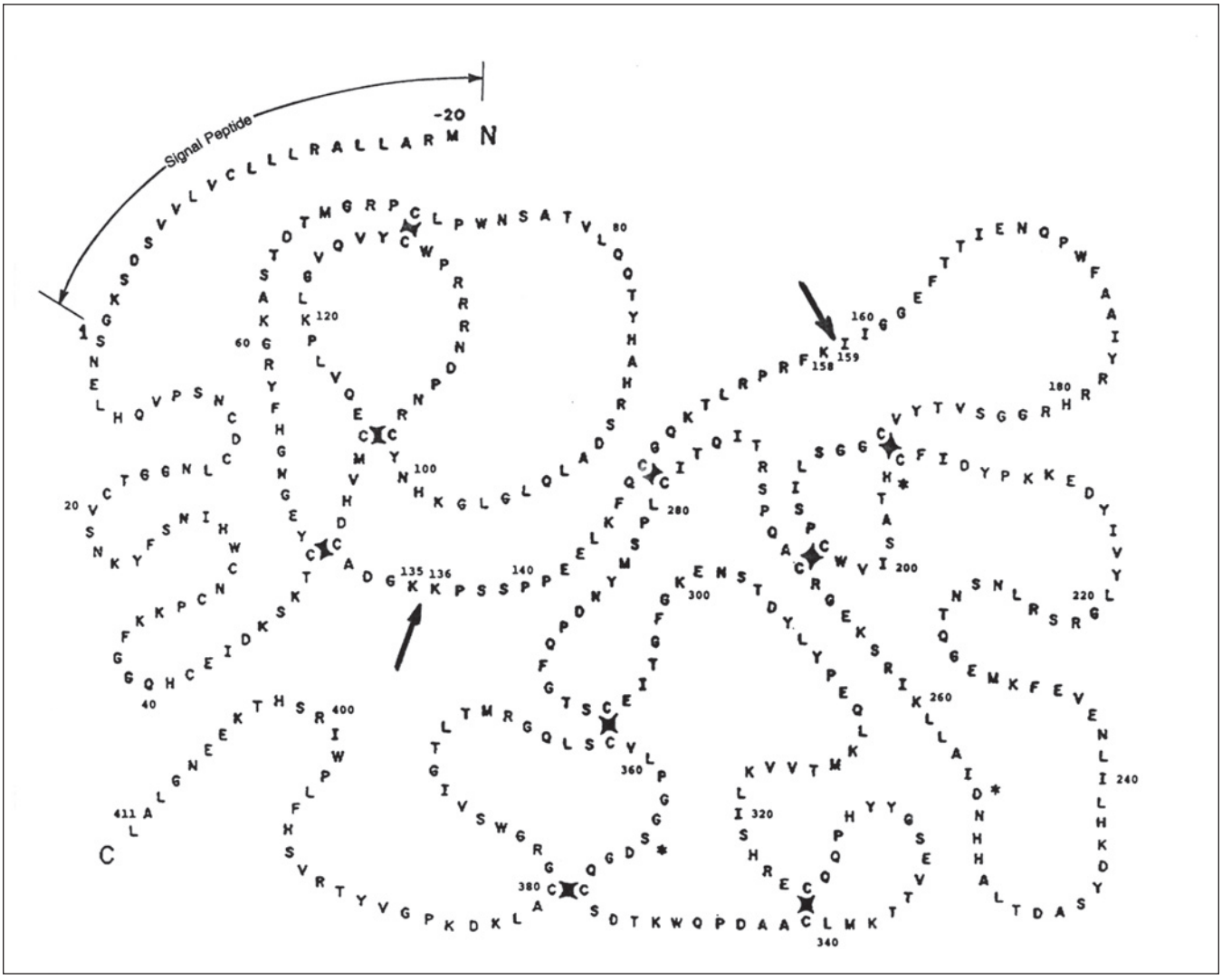

Urokinase is synthesized in this form, called "ScuPA," containing 411 amino acid residues. The enzyme is activated by cleaving at the bonds indicated by the arrows. Antibodies can be tailored to distinguish among the active and inactive forms.

monoclonal antibodies include ones that discriminate between the ScuPA and the HMW form. A combination of these molecular-specific antibodies will enable simultaneous assays of the ScuPA, HMW, and LMW forms in the same specimen of culture medium.

This work was done by Dennis R. Morrison of Johnson Space Center and M. Zouhair Atassi of Baylor College of Medicine. For further information, contact the Johnson Commercial Technology Office at (281) 483-3809.

This invention is owned by NASA, and a patent application has been filed. Inquiries concerning nonexclusive or exclusive license for its commercial development should be addressed to the Patent Counsel, Johnson Space Center, (281) 483-0837. Refer to MSC-21947.

Understanding and Counteracting Fatigue in Flight Crews

Ames Research Center, Moffett Field, California

The materials included in the collection of documents describe the research of the NASA Ames Fatigue Countermeasures Group (FCG), which examines the extent to which fatigue, sleep loss, and circadian disruption affect flight-crew performance. The group was formed in 1980 — in response to a Congressional request to examine a possible safety problem of uncertain magnitude due to transmeridian flying and a potential problem due to fatigue in association with various factors found in air-transport operations — and was originally called the Fatigue/Jet Lag Program. The goals of the FCG are: (1) the development and evaluation of strategies for mitigating the effects of sleepiness and circadian disruption on pilot performance levels; (2) the identification and evaluation of objective approaches for the prediction of alertness changes in flight crews; and (3) the transfer and application of research results to the operational field via classes, workshops, and safety briefings.

Some of the countermeasure approaches that have been identified to be scientifically valid and operationally relevant are brief naps (<40 min) in the cockpit seat and 7-min activity breaks, which include postural changes and ambulation. Although a video-based alertness monitor based on slow eyelid closure shows promise in other operational environments, research by the FCG has demonstrated that in its current form at the time of this reporting, it is not feasible to implement it in the cockpit. Efforts also focus on documenting the impact of untreated fatigue on various types of flight operations. For example, the FCG recently completed a major investigation into the effects of ultra-long-range flights (20 continuous hours in duration) on the alertness and performance of pilots in order to establish a baseline set of parameters against which the effectiveness of new ultra-long-range fatigue remedies can be judged.

This work was done by Melissa Mallis, David Neri, Mark Rosekind, and Philippa Gander of Ames Research Center; John Caldwell of Air Force Research Laboratory; and Curtis Graeber of The Boeing Company. For further information, visit the FCG website at http://human-factors.arc.nasa.gov/zteam.

Inquiries concerning rights for the commercial use of this invention should be addressed to the Ames Technology Partnerships Division at (650) 604-2954. Refer to ARC-15114-1.

Active Correction of Aberrations of Low-Quality Telescope Optics

Relatively inexpensive optical components could be used in free-space optical communications.

NASA's Jet Propulsion Laboratory, Pasadena, California

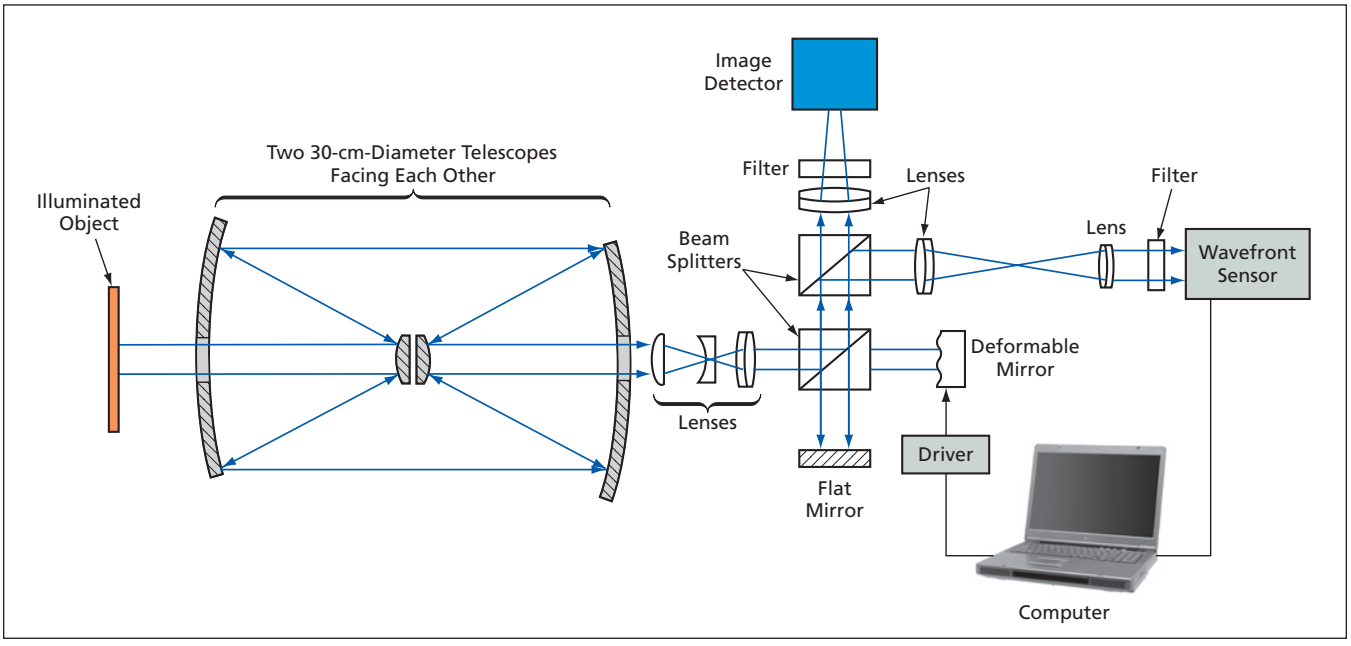

Figure 1. This **Laboratory Apparatus** was used to demonstrate the use of active optics to correct wavefront aberrations introduced by fixed telescope optics.

A system of active optics that includes a wavefront sensor and a deformable mirror has been demonstrated to be an effective means of partly correcting wavefront aberrations introduced by fixed optics (lenses and mirrors) in telescopes. It is envisioned that after further development, active optics would be used to reduce wavefront aberrations of about one wave or less in telescopes having aperture diameters of the order of meters or tens of meters. Although this remaining amount of aberration would be considered excessive in scientific applications in which diffraction-limited performance is required, it would be acceptable for free-space optical-communication applications at wavelengths of the order of 1 μm.

To prevent misunderstanding, it is important to state the following:

- The technological discipline of active optics, in which the primary or secondary mirror of a telescope is directly and dynamically tilted, distorted, and/or otherwise varied to reduce wavefront aberrations, has existed for decades.
- The term "active optics" does not necessarily mean the same thing as does "adaptive optics," even though active optics and adaptive optics are related. The term "adaptive optics" is often used to refer to wavefront correction at speeds characterized by frequencies ranging up to between hundreds of hertz and several kilohertz — high enough to enable mitigation of adverse effects of fluctuations in atmospheric refraction upon propagation of light beams. The term "active optics" usually appears in reference to wavefront correction at significantly lower speeds, characterized by times ranging from about 1 second to as long as minutes.

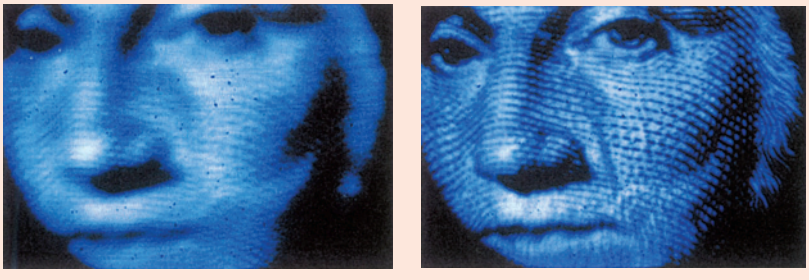

Figure 2. An **Image of Part of a Dollar Bill** was recorded, without and with correction by active optics, in the apparatus of Figure 1.

Hence, the novelty of the present development lies, not in the basic concept of active or adaptive optics, but in the envisioned application of active optics in conjunction with a deformable mirror to achieve acceptably small wavefront errors in free-space optical communication systems that include multi-meter-diameter telescope mirrors that are relatively inexpensive because their surface figures are characterized

by errors as large as about 10 waves. Figure 1 schematically depicts the apparatus used in an experiment to demonstrate such an application on a reduced scale involving a 30-cm-diameter aperture. The apparatus included a source of illumination at a wavelength of 1,064 nm; an object to be imaged (an illuminated dollar bill); two 30-cm amateur astronomical telescopes facing each other to emulate far-field imaging; a 19-element thermally actuated deformable mirror at the pupil plane of the receiving telescope; a Hartmann wavefront sensor; an image detector at the receiving-telescope focal plane; associated lenses, filters, beam splitters; and a flat mirror. The output of the wavefront sensor was processed, by a computer, to control signals for the thermal actuators on the deformable mirror. The lenses were chosen and arranged to reduce the diameter of the light beam to the widths of the deformable mirror and the wavefront sensor. The deformable mirror was placed at the pupil plane of the receiving telescope.

The various optics introduced aberrations characterized by, among other parameters, 1.4 wavelengths of root mean square (RMS) wavefront error. Then the closed-loop control system consisting of the wavefront sensor, computer, and deformable-mirror actuators was turned on, thereby reducing the aberrations (see Figure 2) to 0.05 wavelength RMS wavefront error. In addition, the Strehl ratio (the ratio between the peak intensity in the point spread function of an optical system and that of an equivalent diffraction-limited system) was increased from 0.08 percent to 89 percent.

This work was done by Hamid Hemmati and Yijian Chen of Caltech for NASA's Jet Propulsion Laboratory. Further information is contained in a TSP (see page 1). NPO-43173

Dual-Beam Atom Laser Driven by Spinor Dynamics

A Bose-Einstein condensate is adiabatically compressed to drive coherent spin-mixing evolution.

NASA's Jet Propulsion Laboratory, Pasadena, California

An atom laser now undergoing development simultaneously generates two pulsed beams of correlated ^{87}Rb atoms. (An atom laser is a source of atoms in beams characterized by coherent matter waves, analogous to a conventional laser, which is a source of coherent light waves.) The pumping mechanism of this atom laser is based on spinor dynamics in a Bose-Einstein condensate. By virtue of the angular-momentum conserving collisions that generate the two beams, the number of atoms in one beam is correlated with the number of atoms in the other beam. Such correlations are intimately linked to entanglement and squeezing in atomic ensembles, and atom lasers like this one could be used in exploring related aspects of Bose-Einstein condensates, and as components of future sensors relying on atom interferometry.

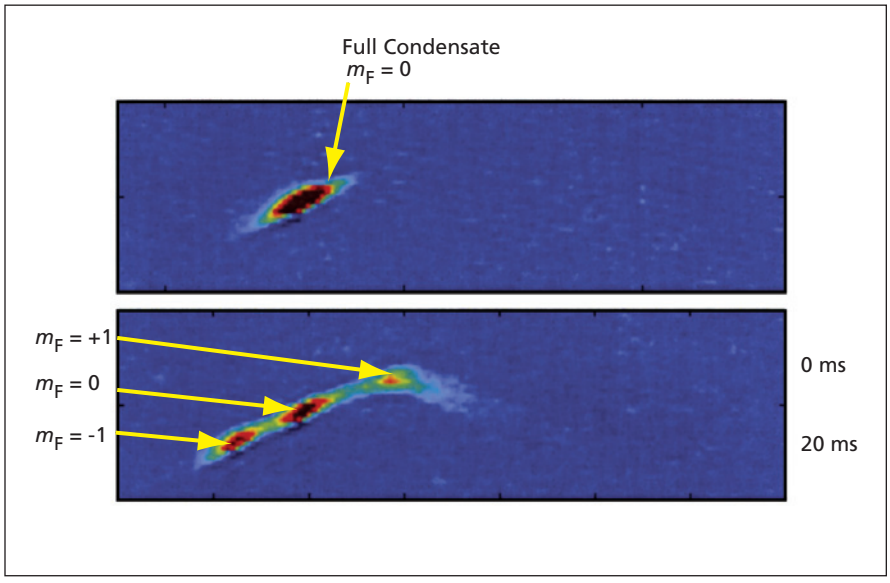

A **Bose-Einstein Condensate of ^{87}Rb** atoms is shown at the instant of turning off the optical trap (0 ms) and at an instant 20 ms later. The original field depicted in these images measures 1 by 0.25 mm. Gravitation was directed toward the lower right; the trapping laser beam was aimed toward the upper right.

In this atom-laser apparatus, a Bose-Einstein condensate of about 2×10^6 ^{87}Rb atoms at a temperature of about 120 μK is first formed through all-optical means in a relatively weak single-beam running-wave dipole trap that has been formed by focusing of a CO_2-laser beam. By a technique that is established in the art, the trap is loaded from an ultrahigh-vacuum magneto-optical trap that is, itself, loaded via a cold atomic beam from an upstream two-dimensional magneto-optical trap that resides in a rubidium-vapor cell that is differentially pumped from an adjoining vacuum chamber, wherein are performed scientific observations of the beams ultimately generated by the atom laser.

In the condensate as thus prepared, the atoms are in the magnetic-field-insensitive $m_F = 0$ sublevel of the F = 1 state [where F is the quantum number of total resultant angular momentum (electron spin plus nuclear spin plus electron orbital angular momentum) and m_F is the quantum number of the component of total resultant angular momentum along a physically distinguishable coordinate axis (typically defined by a magnetic field)]. Then the intensity of the trapping laser beam is increased to drive coherent spin-mixing evolution: The increase in the intensity of the trapping laser beam adiabatically compresses the condensate to cause ^{87}Rb atoms to collide and thereby to undergo the angular-momentum-conserving reaction

$$2(m_F = 0) \leftrightarrow (m_F = +1) + (m_F = -1).$$

As a result of this reaction, the original condensate becomes a superposition of (1) equal numbers of atoms in the $m_F = +1$ and $m_F = -1$ levels and (2) some

other number of atoms in the initial $m_F = 0$ level.

Unlike the $m_F = 0$ level, the $m_F = +1$ and $m_F = -1$ levels are sensitive to an applied magnetic field. Therefore, several milliseconds before turning off the optical trap, a suitably oriented magnetic field having a gradient is turned on. By virtue of their different sensitivities to the magnetic field, atoms in the $m_F = +1$ level can be coupled out of the trap region in one direction and atoms in the $m_F = -1$ level in a different direction (see figure), thereby generating the desired two pulsed beams containing equal numbers of atoms. (The $m_F = 0$ atoms are affected only by the same gravitational force that affects the $m_F = +1$ and $m_F = -1$ atoms.)

This work was done by Robert Thompson, Nathan Lundblad, Lute Maleki, and David Aveline of Caltech for NASA's Jet Propulsion Laboratory. Further information is contained in a TSP (see page 1).
NPO-43741

Rugged, Tunable Extended-Cavity Diode Laser

This laser is relatively insensitive to vibration.

NASA's Jet Propulsion Laboratory, Pasadena, California

A rugged, tunable extended-cavity diode laser (ECDL) has been developed to satisfy stringent requirements for frequency stability, notably including low sensitivity to vibration. This laser is designed specifically for use in an atomic-clock experiment to be performed aboard the International Space Station (ISS). Lasers of similar design would be suitable for use in terrestrial laboratories engaged in atomic-clock and atomic-physics research.

Prior ECDLs, including commercially available ones that were considered for use in the original ISS application, were found to exhibit unacceptably high frequency noise in vibration tests. The high vibration sensitivity of those lasers was attributed to relatively low stiffness of tuning-arm mechanisms, characterized by fundamental-mode vibrational resonance frequencies of ≈2 kHz. In the design of the present ECDL, sensitivity to vibration is increased by increasing stiffness to a point characterized by a fundamental-mode vibrational resonance frequency >6 kHz.

The laser (see figure) includes a laser diode, an optical isolator at the laser output aperture, a collimating-lens assembly, a fixed grating, and a retroreflector prism on a pivoting tuning arm that is driven by a piezoelectric-stack actuator. The tuning arm pivots on flexure blades. The tuning arm and flexure blades are integral to an optical foundation made of Invar (a low-thermal-expansion iron-nickel alloy) and were formed by wire electrical-discharge machining of the foundation. The piezoelectric actuator is held in compressive preload by the flexure blades.

All of the aforementioned components except the flexure blades, tuning arm, and retroreflector are aligned and rigidly mounted within the Invar optical

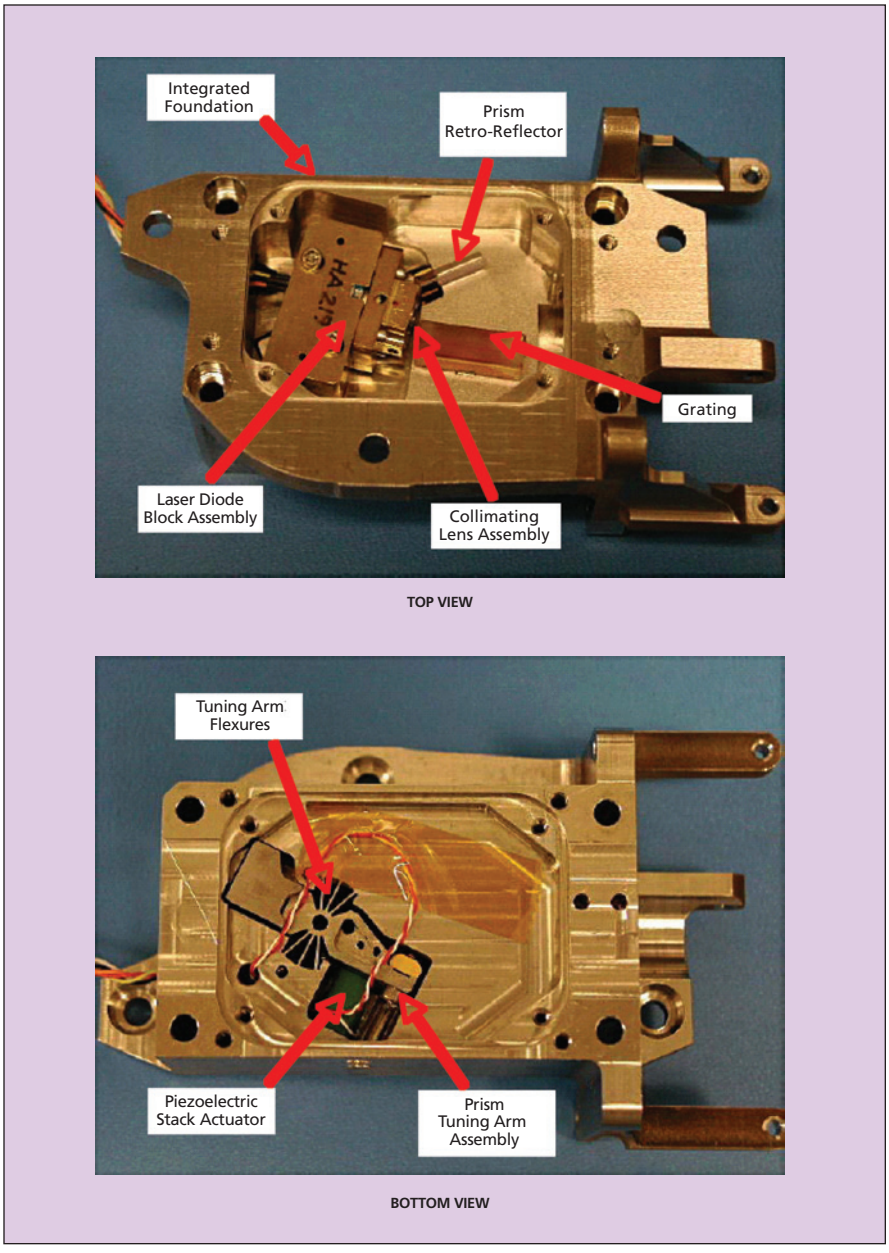

In this **Tunable Extended-Cavity Diode Laser**, tuning is effected by piezoelectric actuation of the tuning arm, which pivots on the flexure blades.

foundation. The laser diode is bonded into a mounting block in such a manner that there is thermal conduction but electrical isolation between the laser-diode case and the optical foundation. The collimating lens is carefully aligned and bonded into the mounting block. The retroreflector prism is bonded to the tuning arm. The tuning arm, the flexures, and the stroke of the piezoelectric actuator were designed to obtain a laser frequency tuning range >125 GHz as well as the vibrational resonance frequency in excess of 6 kHz, while maintaining a minimum compressive load of 1,000 psi (≈6.9 MPa) on the actuator.

This work was done by Donald Moore, David Brinza, David Seidel, and William Klipstein of Caltech and Dong Ho Choi, Lam Le, Guangzhi Zhang, Roberto Iniguez, and Wade Tang of New Focus/Bookham Technology for NASA's Jet Propulsion Laboratory. Further information is contained in a TSP (see page 1).

In accordance with Public Law 96-517, the contractor has elected to retain title to this invention. Inquiries concerning rights for its commercial use should be addressed to:

Innovative Technology Assets Management
JPL
Mail Stop 202-233
4800 Oak Grove Drive
Pasadena, CA 91109-8099
(818) 354-2240
E-mail: iaoffice@jpl.nasa.gov

Refer to NPO-41274, volume and number of this NASA Tech Briefs *issue, and the page number.*

Balloon for Long-Duration, High-Altitude Flight at Venus

A document describes a 5.5-m-diameter, helium-filled balloon designed for carrying a scientific payload having a mass of 44 kg for at least six days at an altitude of about 55 km in the atmosphere of Venus. The requirement for floating at nearly constant altitude dictates the choice of a mass-efficient spherical super-pressure balloon that tracks a constant atmospheric density. Therefore, the balloon is of a conventional spherical super-pressure type, except that it is made of materials chosen to minimize solar radiant heating and withstand the corrosive sulfuric acid aerosol of the Venusian atmosphere.

The shell consists of 16 gores of a multilayer composite material. The outer layer, made of polytetrafluoroethylene, protects against sulfuric acid aerosol. Next is an aluminum layer that reflects sunlight to minimize heating, followed by an aluminized polyethylene terephthalate layer that resists permeation by helium, followed by an aromatic polyester fabric that imparts strength to withstand deployment forces and steady super-pressure. A polyurethane coat on the inner surface of the fabric facilitates sealing at gore-to-gore seams. End fittings and seals, and a tether connecting the end fittings to a gondola, are all made of sulfuric-acid-resistant materials.

This work was done by Jeffrey Hall, Viktor Kerzhanovich, and Andre Yavrouian of Caltech; Debora Fairbrother and Magdi Said of NASA-Wallops Flight Facility; and Chuck Sandy and Thad Fredrickson of ILC Dover, Inc. for NASA's Jet Propulsion Laboratory. Further information is contained in a TSP (see page 1).
NPO-43852

Wide-Temperature-Range Integrated Operational Amplifier

A document discusses a silicon-on-insulator (SOI) complementary metal oxide/semiconductor (CMOS) integrated-circuit operational amplifier to be replicated and incorporated into sensor and actuator systems of Mars-explorer robots. This amplifier is designed to function at a supply potential ≤ 5.5 V, at any temperature from –180 to +120 °C. The design is implemented on a commercial radiation-hard SOI CMOS process rated for a supply potential of ≤ 3.6 V and temperatures from –55 to +110 °C. The design incorporates several innovations to achieve this, the main ones being the following:

- NMOS transistor channel lengths below 1 μm are generally not used because research showed that this change could reduce the adverse effect of hot-carrier injection on the lifetimes of transistors at low temperatures.
- To enable the amplifier to withstand the 5.5-V supply potential, a circuit topology including cascade devices, clamping devices, and dynamic voltage biasing was adopted so that no individual transistor would be exposed to more than 3.6 V.
- To minimize undesired variations in performance over the temperature range, the transistors in the amplifier are biased by circuitry that maintains a constant inversion coefficient over the temperature range.

This work was done by Mohammad Mojarradi, Greg Levanas, Yuan Chen, Elizabeth Kolawa, and Raymond Cozy of Caltech, and Benjamin Blalock, Robert Greenwell, and Stephen Terry of the University of Tennessee for NASA's Jet Propulsion Laboratory. Further information is contained in a TSP (see page 1).

In accordance with Public Law 96-517, the contractor has elected to retain title to this invention. Inquiries concerning rights for its commercial use should be addressed to:

Innovative Technology Assets Management
JPL
Mail Stop 202-233
4800 Oak Grove Drive
Pasadena, CA 91109-8099
(818) 354-2240
E-mail: iaoffice@jpl.nasa.gov

Refer to NPO-42111, volume and number of this NASA Tech Briefs *issue, and the page number.*


NASA
National Aeronautics and
Space Administration